Energy & Environmental Science

PAPER

View Article Online
View Journal

Cite this: DOI: 10.1039/c5ee02066b

A high-performance spectrally-selective solar absorber based on a yttria-stabilized zirconia cermet with high-temperature stability†

Feng Cao,‡[a] Daniel Kraemer,‡[b] Lu Tang,[a] Yang Li,[c] Alexander P. Litvinchuk,[a] Jiming Bao,[c] Gang Chen*[b] and Zhifeng Ren*[a]

Received 5th July 2015,
Accepted 7th September 2015

DOI: 10.1039/c5ee02066b

www.rsc.org/ees

Spectrally-selective solar absorbers are widely used in solar hot water and concentrating solar power (CSP) systems. However, their performance at high temperatures (>450 °C) is still not satisfactory due to high infrared (IR) emittance and lack of long-term thermal stability. Here, we explore yttria-stabilized zirconia (YSZ) cermet-based spectrally-selective surfaces for high-temperature solar absorber applications. The developed multilayer selective surface comprises two sunlight-absorbing W–Ni–YSZ cermet layers with different W–Ni volume fractions inside the YSZ matrix, two anti-reflection coatings (ARCs), and one tungsten IR reflection layer for reduced IR emittance and improved thermal stability, deposited on a polished stainless steel (SS) substrate. The fabricated solar absorbers are tested for their long-term thermal stability at 600 °C. We find a distinct change in the surface morphology of the solar absorbers when oxygen is highly deficient in the YSZ-ARC layers. The oxygen deficiency can be effectively overcome through increasing the oxygen partial pressure during sputtering, which leads to a stable solar absorber with a solar absorptance of ~0.91 and a total hemispherical emittance of ~0.13 at 500 °C. Those values are obtained at the actual operating temperature using an absolute and direct method that measures the total hemispherical emittance with high accuracy. In contrast, most reports on solar absorber development in the literature to date use only near room-temperature spectroscopy techniques that have been shown to significantly underestimate the total hemispherical emittance. This makes our experimentally demonstrated total hemispherical emittance value the lowest ever reported for a high-temperature stable solar absorber with solar absorptance above 0.9.

Broader context

Solar thermal technologies such as solar hot water and concentrating solar power will be a significant part of a sustainable energy solution. To most efficiently convert the sunlight into a terrestrial heat source, spectrally-selective solar absorbers with high solar absorptance and low infrared emittance are needed. Due to the elevated temperatures of solar absorbers during operation not only their photo-thermal performance but also their thermal stability is of great importance for large scale deployment. We report a novel spectrally-selective solar absorber based on a tungsten and nickel filled yttria-stabilized zirconia (YSZ) cermet and explore the effect of oxygen deficiency in YSZ on thermal stability. The optimized solar absorber with minimized oxygen deficiency in the YSZ anti-reflection coating demonstrates a promising thermal stability up to 600 °C, a temperature-independent solar absorptance of ~0.91 and a total hemispherical emittance of ~0.13 directly measured at 500 °C. The here reported total hemispherical emittance is the lowest and most realistic experimentally demonstrated emittance for a spectrally-selective absorber.

Introduction

The sunlight striking the earth is the most abundant renewable energy resource which makes solar thermal technologies one of the promising pathways to meet the rising energy demand while reducing the environmental impact of fossil fuels. Solar thermal technologies convert solar radiation into heat which can be used for domestic hot water systems and industrial processes, or for electricity generation *via* steam turbines[1] and

[a] Department of Physics and TcSUH, University of Houston, Houston, Texas 77204, USA. E-mail: zren@uh.edu
[b] Department of Mechanical Engineering, Massachusetts Institute of Technology, Cambridge, Massachusetts 02139, USA. E-mail: gchen2@mit.edu
[c] Department of Electrical and Computer Engineering, University of Houston, Houston, Texas 77204, USA

† Electronic supplementary information (ESI) available. See DOI: 10.1039/c5ee02066b

‡ Authors contributed equally to this work.

direct energy conversion technologies such as thermoelectric generators (STEGs)[2] and thermophotovoltaics (STPVs).[3,4] In these approaches, instead of using a near blackbody solar receiver, the incorporation of spectrally-selective solar absorbers can enhance the photo-thermal conversion efficiency due to their reduced infrared (IR) emittance paired with high solar absorptance. However, not only the enhanced photo-thermal performance but also the thermal stability at operational temperature is a crucial attribute for high-temperature applications of spectrally-selective solar absorbers.[5] The development of thermally stable high-temperature spectrally-selective solar absorbers which can provide a working fluid at temperatures of 600 °C and above enables a significant increase in the heat engine's conversion efficiency of solar power plants and the integration of solar and natural-gas power plants.[6]

Thus far, a variety of spectrally-selective surfaces have been investigated as mid- and high-temperature solar absorbers such as surfaces based on semiconductor materials with intrinsic spectral selectivity due to a suitable band gap energy from 0.5 to 1.26 eV and multilayer cermet structures comprising a ceramic host with metal filler particles.[7–16] Even though the solar receiver efficiency is only a weak function on the IR emittance at very high optical concentrations,[17] achieving high solar flux densities typically requires complicated and expensive optics. Consequently, minimizing the IR emittance can be advantageous especially at moderate and low solar flux densities. A solar absorber based on $Si_{0.8}Ge_{0.2}$, for example, with a band gap of ~1.04 eV demonstrated a solar absorptance of ~0.90–0.95 while maintaining a relatively low IR emittance of less than 0.3 near the peak of blackbody radiation at 500 °C.[10] Cermet-based solar absorbers have demonstrated high solar absorptance, low IR emittance, and promising thermal stability.[5,18] Commercialized cermet solar absorbers based on W–Al_2O_3, Mo–SiO_2, and Mo–Al_2O_3 have been proven to be stable up to 500 °C. Novel Mo–Si_3N_4 based spectrally selective coatings showed a low total directional emittance of 0.109 at 600 °C which was estimated from a single-angle bidirectional reflectance spectrum measured at room temperature. However, the surfaces showed unsatisfactory thermal stability with a significant increase in emittance to 0.154 (600 °C) after surface annealing at 600 °C in vacuum.[11] In addition, using the single-angle bidirectional reflectance spectrum obtained at room temperature can considerably underestimate the emittance of a spectrally-selective surface at elevated temperatures compared to its true total hemispherical emittance.[19] Al_2O_3-based cermet solar absorbers with Pt as the light absorbing metal filler were suggested to have better thermal stability due to the super antioxidation property of the noble metal.[14,20] However, the use of a noble metal like Pt as filler particles for the cermet layer is rather expensive. In our previous work we reported a W–Ni–Al_2O_3 cermet based spectrally-selective solar absorber with a solar absorptance of ~0.9 on a stainless steel substrate with a tungsten IR reflector layer for a reduced total hemispherical IR emittance of 0.15 at 500 °C that also acts as an elemental diffusion barrier with promising thermal stability at 600 °C in vacuum.[8] A potential challenge for large-scale production of Al_2O_3-based cermet solar absorbers, however, is the slow deposition rate of Al_2O_3 due to relatively high surface binding energy of alumina molecules. In comparison, yttria-stabilized zirconia (YSZ) has a higher deposition rate and has attracted considerable attention for use in solid oxide fuel cells as high-temperature corrosion-resistive coatings, thermal barriers, and optical coatings due to the extraordinary thermal and chemical stability, high refractive index, as well as the transparency in the wavelength range from near IR (NIR) to ultraviolet (UV).[21–24]

In this paper, we explore YSZ as the ceramic host material for a spectrally-selective solar absorber based on a double cermet layer with W and Ni filler metals. We investigate the developed solar absorber in terms of its bidirectional spectral reflectance near room temperature and the directly measured solar absorptance and total hemispherical emittance at temperatures up to 500 °C. We also test the solar absorber for thermal stability at 600 °C in vacuum.

Experimental

Preparation of coatings

All samples are prepared using a commercial magnetron sputtering equipment (AJA International, Inc.). The metals and dielectric materials are deposited by a direct current (DC) and radio frequency (RF) magnetron sputtering, respectively, and the cermet layers are deposited by co-sputtering of the metals and the dielectric host. The multilayer stack includes, the mechanically polished stainless steel (SS) substrate (type: 304, root mean square roughness (R_q): 1.49 nm, dimension: 53 mm × 31.5 mm × 0.762 mm for steady-state calorimetric absorptance and emittance measurements, and 25 mm × 18 mm × 0.762 mm for other measurements), one W IR-reflector layer, two W–Ni–YSZ cermet layers with high and low metal volume fractions in the YSZ ceramic host, and two anti-reflection coating (ARC) layers (YSZ and SiO_2) (Fig. 1). The deposition targets are high purity nickel (99.999%, 2″ Dia.), tungsten (99.95%, 3″ Dia.), YSZ (99.9%, 2″ Dia., ZrO_2/Y_2O_3 92/8 mol%), and SiO_2 (99.995%, 3″ Dia.). The deposition chamber is evacuated to lower than 4×10^{-7} Torr before deposition. The deposition pressure is kept at 3 mTorr. The W IR-reflector layer, the cermet layers, and the SiO_2-ARC layer are deposited in an argon plasma environment. The YSZ-ARC layers are deposited at different oxygen gas flow rates in order to investigate the dependence of the oxygen partial pressure during deposition on the thermal stability of the fabricated surfaces. Additionally, single YSZ layers are directly deposited on SS and sapphire substrates (*C*-plane (0001), 10 mm × 10 mm × 0.5 mm, arithmetic average of absolute value roughness (R_a) < 0.5 nm) at different oxygen partial pressures. The oxygen partial pressure is varied by adjusting the oxygen gas flow rate. At an oxygen gas flow rate of zero the oxygen partial pressure is zero, an oxygen gas flow rate of 2 sccm results in an oxygen partial pressure of 0.2 mTorr, and 4 sccm in 0.375 mTorr. The detailed preparation parameters are summarized in Table 1.

Material characterization and optical measurements

The samples are characterized by performing X-ray diffraction (XRD) measurements using a PANalytical multipurpose diffractometer with an X'Celerator detector and Cu Kα radiation

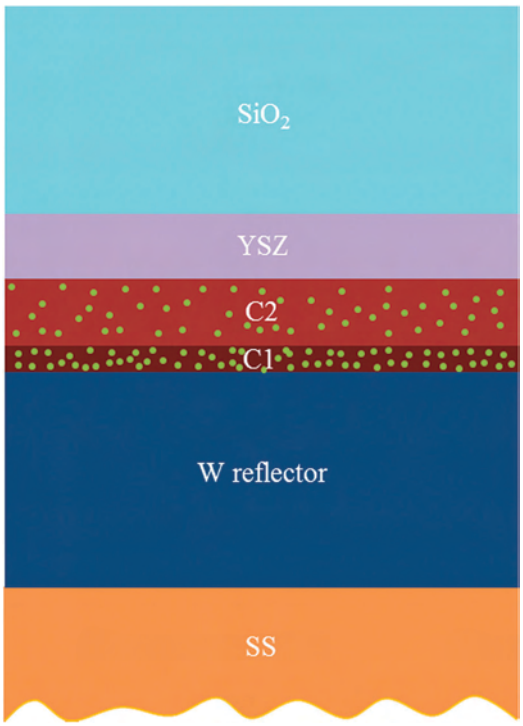

Fig. 1 Schematic of the cermet-based spectrally-selective solar absorber comprising two cermet layers C1 and C2 with different metal volume fractions, two ARC layers (YSZ and SiO_2), and one tungsten IR-reflector layer on a mechanically polished stainless steel (SS) substrate.

(λ = 1.54056 Å) operating at 45 kV and 40 mA. Raman scattering measurements are performed in the back-scattering geometry on a T64000 Raman spectrometer (Horiba Jobin Yvon) at room temperature using an air cooled Ar-ion laser (514 nm) as the excitation source. A Veeco Dimension 3000 Atomic Force Microscope (AFM) is used to characterize the morphology and roughness of the surfaces. The thicknesses of the prepared coatings are measured using an Alpha-step 200 Profilometer (Tencor). The spectral bidirectional reflectance from 0.3 to 1.8 μm is measured using a Cary 500i spectrophotometer with an absolute spectral reflectance accessory at an angle of 8°. The spectral bidirectional reflectance in the wavelength range of 1.8 to 20 μm is recorded on a Nicolet 6700 FT-IR spectrometer using a gold mirror (Thorlabs) as the reference/background sample at an incident angle of 12°. A previously introduced steady-state calorimetric method is used to determine the solar absorptance and total hemispherical emittance at elevated temperatures of up to 500 °C in a vacuum chamber.[19] A sample is attached to an electrical heater assembly and suspended in a vacuum chamber. The electrical input power required to maintain the sample at a steady-state set temperature is recorded. The electrical input power is related to the radiation heat loss from the sample surface and used to obtain the total hemispherical emittance at elevated temperatures. The parasitic heat losses from the heater *via* radiation and lead wire heat conduction are largely minimized by performing a parasitic heat loss calibration measurement. Regarding the solar absorptance, the sample is also attached to an electrical heater assembly and suspended in a vacuum chamber facing a viewport. The sample surface is illuminated with various radiation fluxes from a solar simulator and the electrical input power to the heater assembly is adjusted accordingly to maintain the steady-state set temperature. The solar absorptance is obtained from the change in the electrical power input for a change in the illumination flux. The transmittance spectra of the single YSZ layer coated on sapphire are also recorded on a Cary 500i spectrophotometer. The thermal stability test is carried out in a tubular furnace at 600 °C for 7 days under a vacuum pressure of $\sim 5 \times 10^{-3}$ Torr.

Results and discussion

In order to investigate the effect of oxygen deficiency on the band structure of the YSZ film, we deposit an 80 nm YSZ layer on polished sapphire substrates at different oxygen partial pressures. The transmittance spectra of YSZ layers together with an uncoated sapphire substrate are shown in Fig. 2. The YSZ coatings are transparent down to the wavelength of ~250 nm, where a sharp drop in transmittance is observed which can be explained with an increase in absorption due to the interband transitions of electrons across the band gap.[25] The optical band gap can be extracted from the photon energy dependence of $(\alpha h\nu)^2$ according to the relationship $\alpha \sim \frac{(h\nu - E_g)^q}{h\nu}$, where α is the absorption coefficient, $h\nu$ is the photon energy, E_g is the material's band gap, and the exponent q = 1/2 for a direct band gap material

Table 1 Sputtering parameters of YSZ layers, cermet layers, and optimized spectrally-selective solar absorbers

Sample	Substrate	IR reflector layer	Cermet1	Cermet2	ARC1	ARC2
C1	SS	NA	120 nm	NA	NA	NA
C2	SS	NA	NA	120 nm	NA	NA
YSZ-1	SS or sapphire	NA	NA	NA	80 nm (0 mTorr O_2)	NA
YSZ-2	SS or sapphire	NA	NA	NA	80 nm (0.2 mTorr O_2)	NA
YSZ-3	SS or sapphire	NA	NA	NA	80 nm (0.375 mTorr O_2)	NA
WNY-1	SS	100 nm W	12 nm	30 nm	29 nm (YSZ-1) (0 mTorr O_2)	93 nm
WNY-2	SS	100 nm W	12 nm	30 nm	29 nm (YSZ-2) (0.2 mTorr O_2)	93 nm
WNY-3	SS	100 nm W	12 nm	30 nm	29 nm (YSZ-3) (0.375 mTorr O_2)	93 nm

Tungsten IR reflector layer: W sputtered at a DC power density of 2.2 W cm^{-2}. Cermet1: W–Ni–YSZ sputtered with a DC power density of 0.33 W cm^{-2} for W and 0.99 W cm^{-2} for Ni, and a RF power density of 7.4 W cm^{-2} for YSZ. Cermet2: W–Ni–YSZ sputtered with a DC power density of 0.26 W cm^{-2} for W and 0.74 W cm^{-2} for Ni, and a RF power density of 7.4 W cm^{-2} for YSZ. ARC1: YSZ sputtered with a RF power density of 7.4 W cm^{-2} with different oxygen partial pressures. ARC2: SiO_2 sputtered with a RF power density of 4.4 W cm^{-2}.

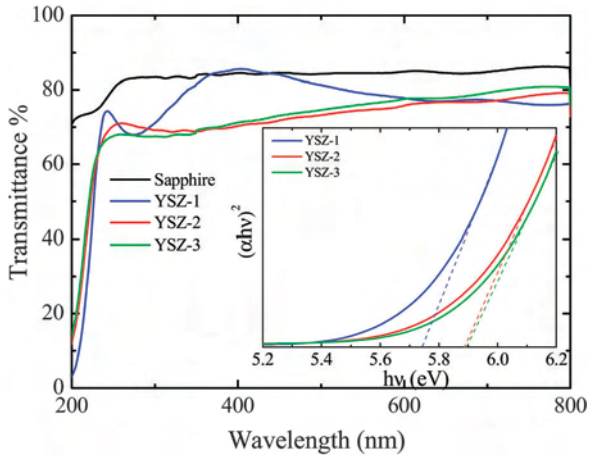

Fig. 2 Ultraviolet-visible (UV-Vis) transmittance spectra of a single layer of YSZ coatings deposited on a sapphire single crystal substrate (*C*-plane, (0001)) with different oxygen partial pressures in the deposition process. The inset shows the plot of $(\alpha h\nu)^2$ *vs.* photon energy for YSZ films. (α: absorption coefficient).

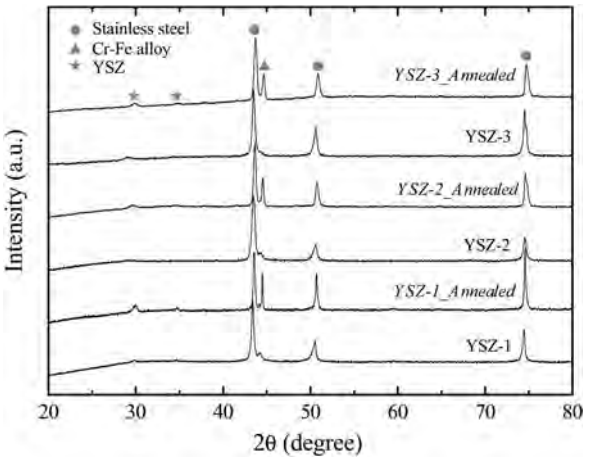

Fig. 3 XRD patterns of a single YSZ layer deposited on SS substrates with different oxygen partial pressures before and after annealing at 600 °C for 7 days. (YSZ-1, 0 mTorr oxygen partial pressure; YSZ-2, 0.2 mTorr oxygen partial pressure; and YSZ-3, 0.375 mTorr oxygen partial pressure).

(inset of Fig. 2).[26] The band gap of YSZ-1 (zero oxygen partial pressure) is $\sim 5.74 \pm 0.03$ eV, which is in the range of reported YSZ films (5.4–5.9 eV).[25–27] Upon increasing the oxygen partial pressure in the deposition process, the band gap energy increases by ~ 0.15 eV due to the suppression of localized defect states formed by the oxygen vacancies in the zirconia lattice.[25] The observation indicates that the band gap decreases with increasing oxygen deficiency resulting from the recombination of atomic oxygen to molecular oxygen in sole argon plasma.[22]

The single YSZ-ARC layers (YSZ-1, YSZ-2, and YSZ-3) are also deposited on SS to investigate the effect of the solar absorber substrate on the YSZ layer. The as-deposited YSZ layers show two weak peaks related to the YSZ phase marked with filled stars in the XRD patterns (Fig. 3).[28] The films deposited at ambient temperature are partially crystallized. This is different from other dielectric films, such as SiO_2 and Al_2O_3, prepared with the same procedures exhibiting an amorphous nature. Other peaks marked with filled circles and filled triangles can be attributed to the SS substrate. The YSZ thin film further crystallizes during a high temperature annealing process as indicated by the more pronounced YSZ peaks in the annealed samples. The three single YSZ layers experience a similar morphology change upon annealing which manifests itself with an increase in particle size and roughness (Fig. S1, ESI†). The change in roughness, however, is less pronounced with an increase from 6–7 nm to 8–10 nm.

The solar absorbers (WNY-1, WNY-2, and WNY-3) with different YSZ ARC layers obtained at different oxygen partial pressures (Table 1) are used to study the effect of oxygen deficiency in the YSZ ARC layer on the spectral selectivity and thermal stability of the solar absorber. The resulting bidirectional reflectance spectra of the solar absorbers are shown in Fig. 4. The spectral reflectance below 1.1 μm is relatively small in all the as-deposited samples, which is due to the particular configuration of the double cermet layers and double ARC layers. The sharp

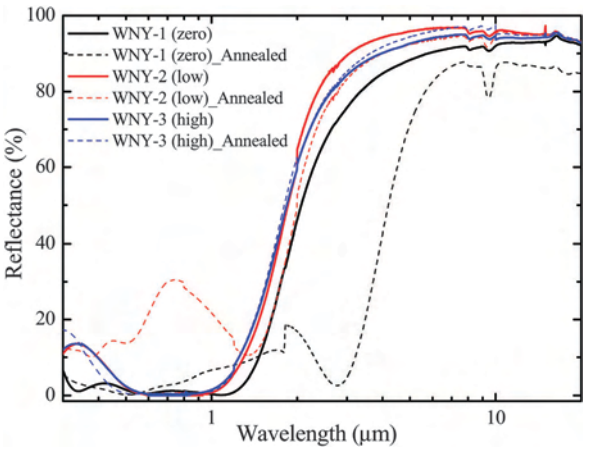

Fig. 4 Bidirectional reflectance spectra of solar absorbers deposited with different oxygen partial pressures (black line: WNY-1 (zero), 0 mTorr oxygen partial pressure; red line: WNY-2 (low), 0.2 mTorr oxygen partial pressure; blue line: WNY-3 (high), 0.375 mTorr oxygen partial pressure) in the process of depositing a YSZ ARC layer before (solid lines) and after (dash lines) annealing at 600 °C for 7 days.

transition from low to high spectral reflectance occurs in the wavelength range of ~ 1 μm to 3 μm, which indicates a low spectral emittance above 3 μm induced by the tungsten IR-reflector layer. With reduced oxygen deficiency (films deposited at higher oxygen partial pressures), the spectral reflectance increases in both the UV and IR wavelength regions and the transition shifts to a shorter wavelength, possibly due to the decreasing optical thickness of the YSZ ARC layer.[25] The selective surfaces are deposited on an opaque mechanically polished SS substrate with roughness smaller than 10 nm supporting the assumption of no diffuse reflection. Therefore, the spectral bidirectional reflectance, ρ_λ', can be used to calculate the spectral directional absorptance, $\alpha_\lambda' = \varepsilon_\lambda' = 1 - \rho_\lambda'$, which is equivalent to the spectral directional emittance, ε_λ'. Also, it has been shown that the spectral bidirectional reflectance of cermet-based selective surfaces exhibits only a weak angular

dependence up to ~60°.[29] Thus, the small difference in the measurement angles between the UV-Vis-NIR spectrophotometer (8°) and the FT-IR spectrometer (12°) does not significantly affect the measured bidirectional reflectance spectra permitting the combination of the two spectra with negligible error. However, the results of the spectral bidirectional reflectance measurement should only be used for quick sample screening due to many shortcomings of that measurement technique which we later discuss in detail. Also, in the case of thermally unstable samples that undergo an increase in surface roughness upon annealing the possible increase in diffuse reflection adds further uncertainties. Nevertheless, assuming temperature-independent bidirectional reflectance spectra the near normal solar absorptance and total directional emittance can be estimated by integrating the combined directional absorptance spectra (0.3–20 μm) weighted by the solar and blackbody spectra, respectively. The observed changes in the bidirectional reflectance spectra manifest themselves as decreasing near normal solar absorptance and total directional emittance with increasing oxygen partial pressure (Table 2). Upon annealing in vacuum for 7 days at 600 °C significant changes in the reflectance spectra are observed for the absorbers with the YSZ-ARC layers deposited at zero and low oxygen partial pressures (WNY-1 and WNY-2). An increase of the emittance on WNY-1 is caused by the degradation of the W IR-reflector layer. The decreasing absorptance of the WNY-2 sample indicates the degradation of the cermet absorption layers. The solar absorptance and thermal emittance are most stable for the sample (WNY-3) with the YSZ-ARC layer deposited at the highest oxygen partial pressure. This YSZ-ARC layer may be fully oxidized and hence suppresses the elemental diffusion of metals into and within the cermet layers. Consequently, the developed spectrally-selective solar absorber shows great promise for use in high temperature solar thermal applications.

In order to understand the observed changes in the optical properties of the fabricated solar absorbers (Fig. 4) we investigated the possible degradation mechanisms occurring during the high temperature annealing process. It has been shown that changes in the surface morphology can be responsible for changing the radiative properties at high temperatures.[5,30] We indeed observe significant changes in surface morphologies in terms of surface roughness and average particle size upon high-temperature annealing for the solar absorbers with the YSZ layers deposited at zero and 0.2 mTorr oxygen partial pressures (Fig. 5). The root mean square roughness (R_q) increases from 8–11 nm to 15–18 nm, and the average particle size increases from ~70 nm to 300–500 nm. The initial groove structure created by the mechanical polishing process of the stainless steel substrate disappears upon annealing due to the diffusion and growth of particles (Fig. 5(a)–(d)). Only for the solar absorber prepared with the YSZ ARC layer deposited at high oxygen partial pressure (0.375 mTorr) changes in the surface morphology are suppressed (Fig. 5(e) and (f)). Similar observations were made with our recently reported W–Ni–Al_2O_3 cermet based solar absorber.[8] The cause for the changes in the surface morphology can possibly be linked to the oxygen deficiency in the YSZ host of the cermet layers and in the YSZ ARC layer which leads to a larger number density of vacancies and stress within the layers. Both vacancies and stress promote diffusion processes within the layers at high temperature leading to the observed accelerated deformation of the surfaces. However, depositing the YSZ ARC layer at a high enough oxygen partial pressure yields a fully oxidized YSZ which is proven to be a thermally stable high temperature ceramics and thus, can suppress the surface deformation and the changes in the optical properties suggesting promising high-temperature stability.

Even though we have demonstrated that W can be used as an excellent high-temperature diffusion barrier layer between a SS substrate and cermet layers in a previous publication, the diffusion of atoms is inevitable over time. Thus, it might be of interest to explore the properties of the new cermet material (W–Ni–YSZ) by analyzing the morphology and phase change upon annealing of a cermet layer directly deposited on a SS substrate. Before annealing XRD patterns of the single cermet layers with different metal volume fractions in YSZ on SS (C1 and C2) show sharp diffraction peaks from the SS substrate (Fig. 6a). However, after annealing the XRD patterns display Cr–Fe alloy peaks due to insufficient oxidation of Cr metal at the oxide–metal interface,[31] and additional small peaks of the $FeWO_4$ phase resulting from the reaction of diffused Fe from SS and W in the residual oxygen environment.[8,12] The presence of the $FeWO_4$ phase is also seen in the Raman spectra (Fig. 6b), which have two distinct Raman peaks at 882 cm^{-1} and 691 cm^{-1} for the annealed cermet samples (C1 and C2) caused by the A_g modes of the $FeWO_4$ phase.[32] Therefore, the diffusion of Fe atoms cannot be suppressed by switching from Al_2O_3 to YSZ as the host material. In addition to the $FeWO_4$ phase we also observe a $FeCr_2O_4$ phase in the annealed cermet samples resulting from the oxidation of the SS substrate during long-term annealing at 600 °C.[33] The roughness (R_q) increases from 7–9 nm to 34–37 nm and the particle size increases from ~50 nm to 300–400 nm (Fig. 7). This leads to a conclusion that the YSZ-based cermet layer deposited onto a SS substrate without an interstitial diffusion barrier (100 nm W layer) and a top ARC protective layer cannot survive the 7 day annealing process at 600 °C in vacuum.

The spectral bidirectional reflectance measurement is a useful and quick tool to screen the developed solar absorbers. However, to determine to what extent the solar absorptance is dependent on the operating temperature of the solar absorber and to obtain a more realistic value for the total-hemispherical emittance we use a previously developed steady-state calorimetric method

Table 2 The estimated solar absorptance (solar spectrum (AM 1.5 direct + circumsolar) weighted integration of bidirectional reflectance spectra) and total-directional emittance (integration of bidirectional reflectance spectra weighted by the blackbody spectrum at 82 °C and 500 °C) of prepared solar absorbers before and after annealing at 600 °C for 7 days in vacuum

	Before annealing			After annealing		
		Emittance			Emittance	
Sample	Absorptance	82 °C	500 °C	Absorptance	82 °C	500 °C
WNY-1	95.5%	8.2%	15.0%	95.7%	16.0%	40.9%
WNY-2	93.0%	4.4%	7.1%	77.7%	5.8%	10.8%
WNY-3	92.7%	5.9%	10.1%	93.0%	4.5%	8.5%

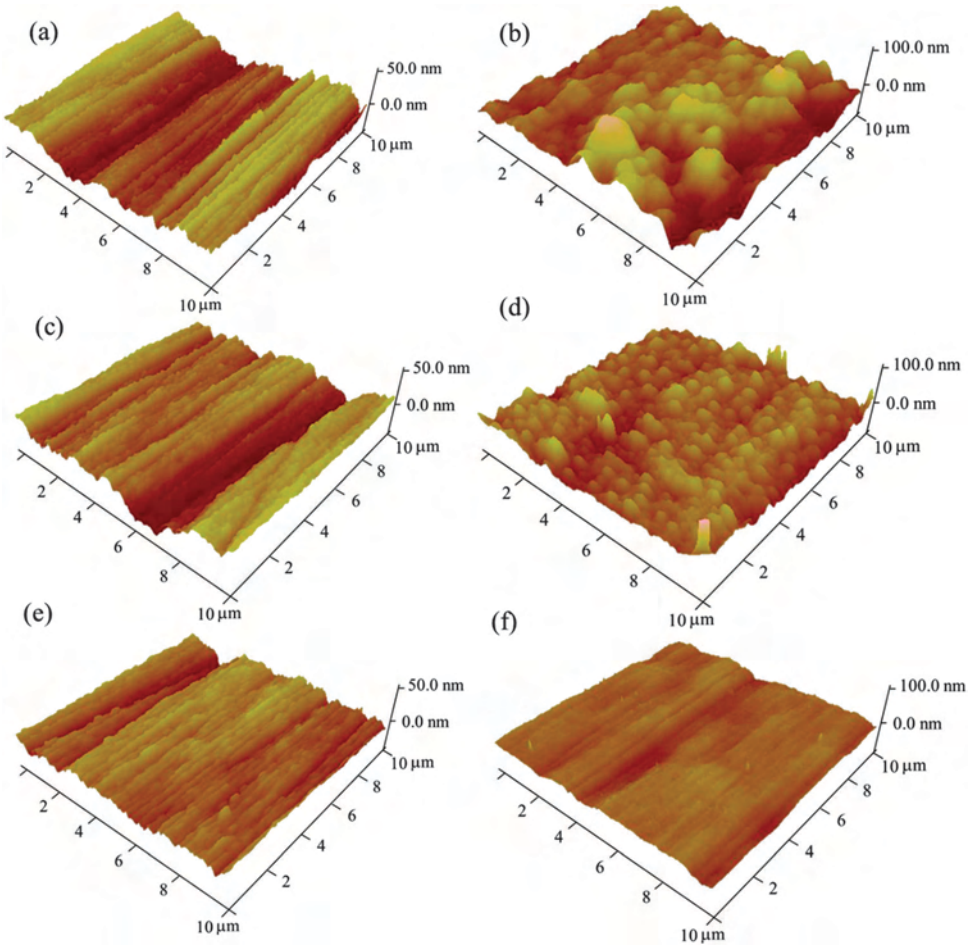

Fig. 5 AFM images of solar absorbers with zero oxygen partial pressure before (a) and after (b) annealing, 0.2 mTorr oxygen partial pressure before (c) and after (d) annealing and 0.375 mTorr oxygen partial pressure before (e) and after (f) annealing at 600 °C for 7 days.

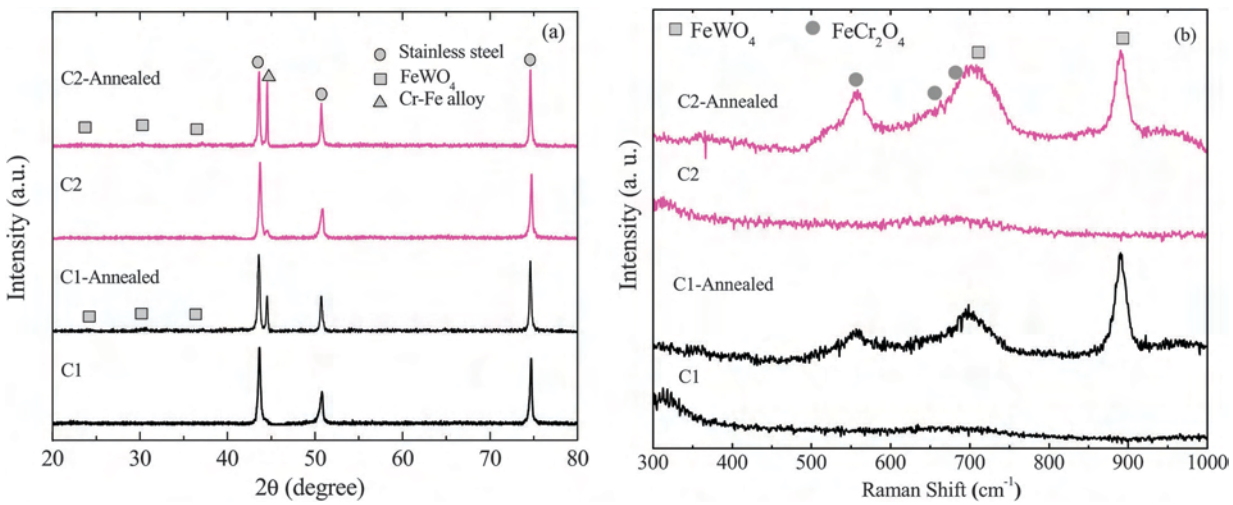

Fig. 6 The XRD patterns (a) and Raman spectra (b) of cermet coatings with a high metal volume fraction (C1) and a low metal volume fraction (C2) in the YSZ matrix before and after annealing at 600 °C for 7 days.

(briefly described in the Experimental section).[19] For the most promising solar absorber sample (WNY-3), we measure a temperature-independent solar absorptance of ~0.91 up to 500 °C (Fig. 8) which is close to the solar absorptance calculated from spectral bidirectional reflectance data shown in Table 2. The total hemispherical emittance of 0.13 at 500 °C (Fig. 8) is

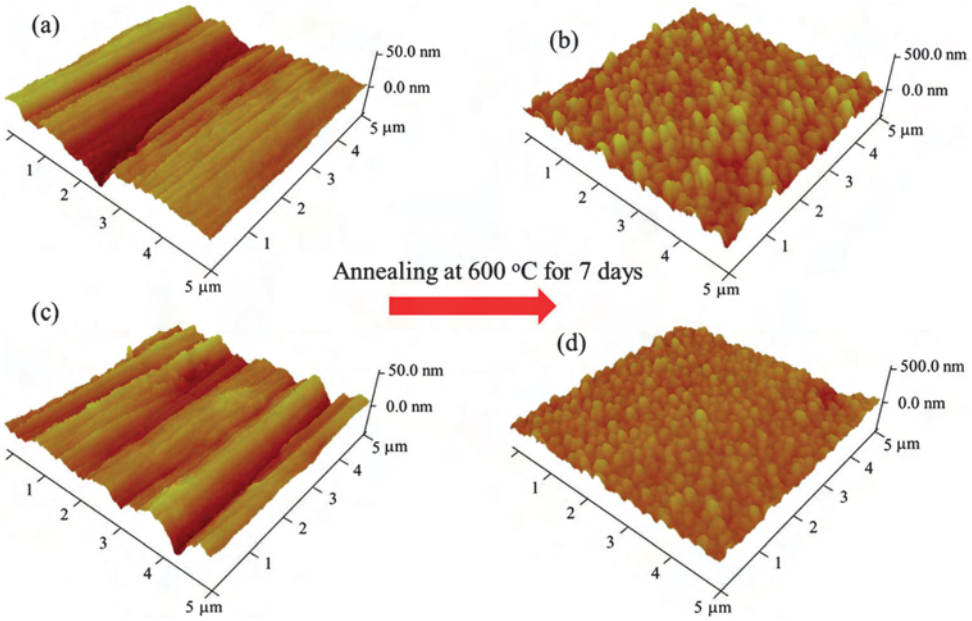

Fig. 7 AFM images of cermets deposited on SS substrates with a high metal volume fraction in the YSZ matrix before (a) and after (b) annealing and a low metal volume fraction in the YSZ matrix before (c) and after (d) annealing at 600 °C for 7 days.

almost 30% higher than that expected from the value calculated from the bidirectional spectral data at room temperature and the blackbody spectrum at 500 °C. The origin of this discrepancy lies with the inaccuracies in obtaining the emittance from a spectral reflectance measurement of a highly reflective sample. A small relative error in the reflectance translates into a proportionally larger error in the calculated emittance. Additionally, a significant difference in the two values is expected because the spectral reflectance is measured only at one angle and at room temperature which assumes specular reflection is dominated, and ignores the angular dependence of the reflectance and the temperature dependence of the materials' dielectric functions. These assumptions lead to a significant underestimation of the sample's emittance because the emissivity of metal (mostly responsible for the absorber's IR emittance) increases with increasing polar angle and temperature.[34] The total hemispherical emittance expectedly increases with temperature due to the shift of the blackbody spectrum to a shorter wavelength with increasing temperature and due to the temperature dependence of the optical properties. In spite of the discrepancies, a very competitive IR emittance of 0.13 is demonstrated at 500 °C (Fig. 8). Thus far, most research on the development of solar absorbers obtained the solar absorptance and IR emittance using the data from near room-temperature spectroscopy techniques with the above-described shortcomings. Therefore, to the best of our knowledge this is the lowest experimentally demonstrated total hemispherical emittance to date for a spectrally-selective solar absorber with a solar absorptance larger than 0.9 and promising high-temperature stability. As illustrated in Fig. 8, the developed solar absorber based on a YSZ host material represents an improvement in terms of an increase in solar absorptance by 0.05 as well as a reduction in IR emittance by 0.02 at 500 °C

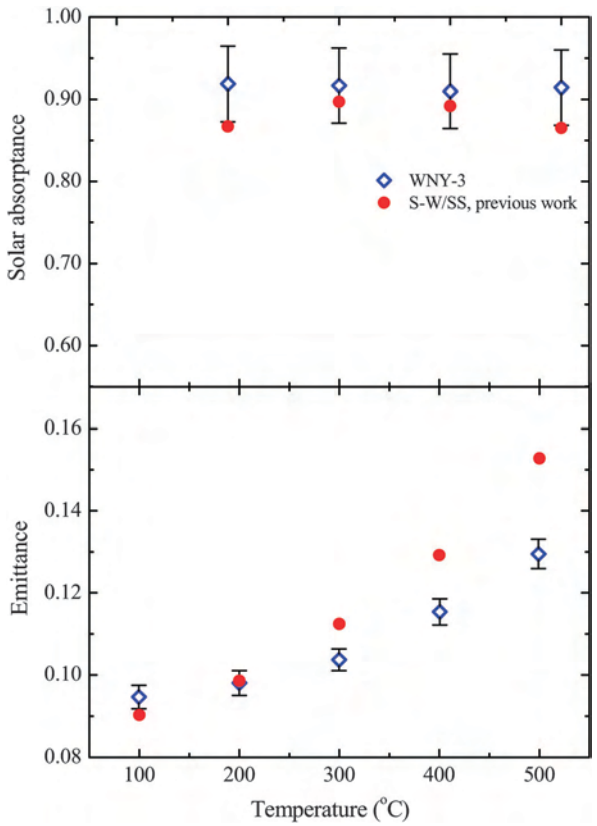

Fig. 8 Temperature dependence of the near normal solar absorptance and total hemispherical emittance of a solar absorber deposited with 0.375 mTorr oxygen partial pressure during the deposition process of the YSZ ARC layer (WNY-3) measured using a direct steady-state calorimetric method (blue open circles). For comparison, the data for the W–Ni–Al_2O_3 cermet based solar absorber (S-W/SS) are included (red solid circles).[8]

compared to our previously reported W–Ni–Al_2O_3 cermet based solar absorber.[8] Even though those improvements might seem incremental, they have a considerable effect on the photothermal conversion efficiency of a solar thermal device.[18]

Conclusions

In conclusion, we developed a W–Ni–YSZ cermet-based spectrally-selective solar absorber on polished SS for potential high temperature solar thermal applications. Changes in the optical properties of the solar absorbers upon annealing are due to the changing surface morphology which is possibly caused by metal diffusion into an oxygen deficient YSZ ARC layer. This diffusion and morphology change can be suppressed by depositing the YSZ ARC layer at high oxygen partial pressures to ensure full oxidation of YSZ and thermal stability at high temperatures. The optimized spectrally-selective solar absorber based on a W–Ni–YSZ cermet with a W IR-reflector as a diffusion barrier deposited on a stainless steel substrate shows great promise to be stable in vacuum up to 600 °C. The demonstrated solar absorber exhibits a temperature-independent solar absorptance of $\sim$0.91 and a total hemispherical emittance of $\sim$0.13 directly measured at 500 °C. We show that the IR emittance calculated in the conventional way from near room-temperature spectral directional reflectance data significantly underestimates the total hemispherical emittance of a spectrally-selective solar absorber at elevated temperatures. Thus, we can say that to the best of our knowledge this is the lowest experimentally demonstrated total hemispherical emittance to date for a spectrally-selective solar absorber with a solar absorptance larger than 0.9 and promising high-temperature stability. In addition to the improved performance compared to our previously developed Al_2O_3-based cermet solar absorber, the significantly higher deposition rates of YSZ compared to Al_2O_3 suggests the advantage of higher production rates.

Acknowledgements

This work was supported by ''Solid State Solar-Thermal Energy Conversion Center (S^3TEC)'', an Energy Frontier Research Center funded by the U.S. Department of Energy, Office of Science, and Office of Basic Energy Science under award number DE-SC0001299/DE-FG02-09ER46577 (GC and ZFR) and ''Concentrated Solar Thermoelectric Power (CSP)'', DOE SunShot CSP grant, under award number DE-EE0005806. J.M.B acknowledges support from National Science Foundation (Career Award ECCS-1240510) and the Robert A. Welch Foundation (E-1728).

Notes and references

1 D. Mills, *Sol. Energy*, 2004, **76**, 19–31.
2 D. Kraemer, B. Poudel, H. P. Feng, J. C. Caylor, B. Yu, X. Yan, Y. Ma, X. W. Wang, D. Z. Wang, A. Muto, K. McEnaney, M. Chiesa, Z. F. Ren and G. Chen, *Nat. Mater.*, 2011, **10**, 532–538.
3 F. Mauthner and W. Weiss, *Solar Heat Worldwide*, Solar Heating & Cooling Programme International Energy Agency, 2013.
4 N. Wang, L. Han, H. C. He, N. H. Park and K. Koumoto, *Energy Environ. Sci.*, 2011, **4**, 3676–3679.
5 C. E. Kennedy, *Review of Mid to High Temperature Solar Selective Absorber Materials*, National Renewable Energy Laboratory, 2002.
6 S. Chu and A. Majumdar, *Nature*, 2012, **488**, 294–303.
7 J. Moon, T. K. Kim, B. VanSaders, C. Choi, Z. Liu, S. Jin and R. Chen, *Sol. Energy Mater. Sol. Cells*, 2015, **134**, 417–424.
8 F. Cao, D. Kraemer, T. Sun, Y. Lan, G. Chen and Z. Ren, *Adv. Energy Mater.*, 2015, **5**, 1401042.
9 X. Yu, X. Wang, Q. Zhang, J. Li and J. Liu, *J. Appl. Phys.*, 2014, **116**, 073508.
10 J. Moon, D. Lu, B. VanSaders, T. K. Kim, S. D. Kong, S. Jin, R. Chen and Z. Liu, *Nano Energy*, 2014, **8**, 238–246.
11 E. Céspedes, M. Wirz, J. A. Sánchez-García, L. Alvarez-Fraga, R. Escobar-Galindo and C. Prieto, *Sol. Energy Mater. Sol. Cells*, 2014, **122**, 217–225.
12 J. Cheng, C. Wang, W. Wang, X. Du, Y. Liu, Y. Xue, T. Wang and B. Chen, *Sol. Energy Mater. Sol. Cells*, 2013, **109**, 204–208.
13 X. X. Wang, H. F. Li, X. B. Yu, X. L. Shi and J. F. Liu, *Appl. Phys. Lett.*, 2012, **101**, 203109.
14 Z. Y. Nuru, C. J. Arendse, R. Nemutudi, O. Nemraoui and M. Maaza, *Phys. B*, 2012, **407**, 1634–1637.
15 J. A. Wang, B. C. Wei, Q. R. Wei and D. J. Li, *Phys. Status Solidi A*, 2011, **208**, 664–667.
16 A. Antonaia, A. Castaldo, M. L. Addonizio and S. Esposito, *Sol. Energy Mater. Sol. Cells*, 2010, **94**, 1604–1611.
17 K. McEnaney, Master thesis, Massachusetts Institute of Technology, 2010.
18 F. Cao, K. McEnaney, G. Chen and Z. Ren, *Energy Environ. Sci.*, 2014, **7**, 1615–1627.
19 D. Kraemer, K. McEnaney, F. Cao, Z. Ren and G. Chen, *Sol. Energy Mater. Sol. Cells*, 2015, **132**, 640–649.
20 H. G. Craighead, R. E. Howard, J. E. Sweeney and R. A. Buhrman, *Appl. Phys. Lett.*, 1981, **39**, 29–31.
21 P. Amezaga-Madrid, A. Hurtado-Macias, W. Antunez-Flores, F. Estrada-Ortiz, P. Piza-Ruiz and M. Miki-Yoshida, *J. Alloys Compd.*, 2012, **536**, S412–S417.
22 D. E. Ruddell, B. R. Stoner and J. Y. Thompson, *Thin Solid Films*, 2003, **445**, 14–19.
23 S. Venkataraj, O. Kappertz, H. Weis, R. Drese, R. Jayavel and M. Wuttig, *J. Appl. Phys.*, 2002, **92**, 3599–3607.
24 P. Scardi, L. Lutterotti and E. Galvanetto, *Surf. Coat. Technol.*, 1993, **61**, 52–59.
25 S. Heiroth, R. Ghisleni, T. Lippert, J. Michler and A. Wokaun, *Acta Mater.*, 2011, **59**, 2330–2340.
26 I. Kosacki, V. Petrovsky and H. U. Anderson, *Appl. Phys. Lett.*, 1999, **74**, 341–343.
27 N. Nicoloso, A. Lobert and B. Leibold, *Sens. Actuators, B*, 1992, **8**, 253–256.
28 S. Heiroth, R. Frison, J. L. M. Rupp, T. Lippert, E. J. B. Meier, E. M. Gubler, M. Dobeli, K. Conder, A. Wokaun and L. J. Gauckler, *Solid State Ionics*, 2011, **191**, 12–23.

29 A. Sakurai, H. Tanikawa and M. Yamada, presented in part at the 7th International Symposium on Radiative Transfer, Kusadasi, June, 2013.
30 M. Nishimura and T. Ishiguro, *Jpn. J. Appl. Phys.*, 2004, **43**, 757–761.
31 A. Visnapuu, J. S. Volosin and R. B. Schluter, Annealing study of stainless steel to conserve critical metals, Report of investigations/1994, 1994.
32 J. Ruiz-Fuertes, D. Errandonea, S. López-Moreno, J. González, O. Gomis, R. Vilaplana, F. J. Manjón, A. Muñoz, P. Rodríguez-Hernández, A. Friedrich, I. A. Tupitsyna and L. L. Nagornaya, *Phys. Rev. B: Condens. Matter Mater. Phys.*, 2011, **83**, 214112.
33 S. Inoue, H. Uchida, M. Morii and K. Koterazawa, *J. Jpn. Inst. Met.*, 1990, **54**, 1376–1381.
34 M. Q. Brewster, *Thermal radiative transfer and properties*, John Wiley & Sons, 1992.